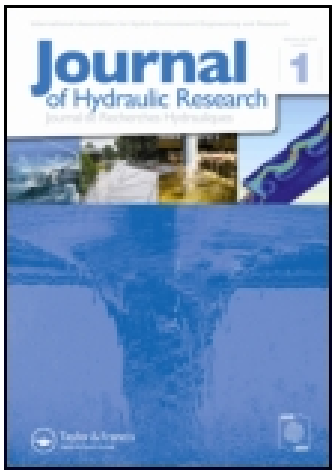

Journal of Hydraulic Research
Publication details, including instructions for authors and subscription information:
http://www.tandfonline.com/loi/tjhr20

Scale effects in physical hydraulic engineering models

Valentin Heller [a]
[a] School of Civil Engineering and the Environment , University of Southampton , Highfield, Southampton, SO17 1BJ, UK
Published online: 17 Jun 2011.

To cite this article: Valentin Heller (2011) Scale effects in physical hydraulic engineering models, Journal of Hydraulic Research, 49:3, 293-306, DOI: 10.1080/00221686.2011.578914

To link to this article: http://dx.doi.org/10.1080/00221686.2011.578914

IAHR AIRH
Taylor & Francis
Taylor & Francis Group

Journal of Hydraulic Research Vol. 49, No. 3 (2011), pp. 293–306
doi:10.1080/00221686.2011.578914

Forum paper

Scale effects in physical hydraulic engineering models

VALENTIN HELLER (IAHR Member), Research Fellow, *School of Civil Engineering and the Environment, University of Southampton, Highfield, Southampton SO17 1BJ, UK.*
Email: v.heller@soton.ac.uk

ABSTRACT
Scale effects arise due to force ratios which are not identical between a model and its real-world prototype and result in deviations between the up-scaled model and prototype observations. This review article considers mechanical, Froude and Reynolds model–prototype similarities, describes scale effects for typical hydraulic flow phenomena and discusses how scale effects are avoided, compensated or corrected. Four approaches are addressed to obtain model–prototype similarity, to quantify scale effects and to define limiting criteria under which they can be neglected. These are inspectional analysis, dimensional analysis, calibration and scale series, which are applied to landslide generated impulse waves. Tables include both limiting criteria to avoid significant scale effects and typical scales of physical hydraulic engineering models for a wide variety of hydraulic flow phenomena. The article further shows why it is challenging to model sediment transport and distensible structures in a physical hydraulic model without significant scale effects. Possible future research directions are finally suggested.

Keywords: Dimensional analysis, Froude similarity, landslide generated impulse wave, physical hydraulic modelling, Reynolds similarity, scale effect, scale series, similarity theory

1 Introduction

A physical hydraulic model represents a real-world prototype and is used as a tool for finding technically and economically optimal solutions of hydraulic engineering problems (Novak 1984). Considerable differences between up-scaled model and prototype parameters may result due to model, scale and/or measurement effects. *Model effects* (Yalin 1971, Ivicsics 1978, Bretschneider, in Kobus 1980, Novak 1984, Hughes 1993) originate from the incorrect reproduction of prototype features such as geometry (2D modelling or reflections), flow or wave generation techniques (turbulence intensity level in approach flow or linear wave approximation) or fluid properties (number of nuclei for cavitation or fresh instead of sea water). *Scale effects* (Yalin 1971, Le Méhauté 1990, Hughes 1993, Martin and Pohl 2000, Heller 2007) arise due to the inability to keep each relevant force ratio constant between the scale model and its real-world prototype. *Measurement effects* (Schüttrumpf and Oumeraci 2005) include non-identical measurement techniques used for data sampling in the model and prototype (intruding vs. non-intruding measurement system or different probe sizes).

The estimation of how model, scale or measurement effects qualitatively and quantitatively affect the model results and whether or not they can be neglected is a challenge for physical modellers. Numerical simulations may be able to consider model effects, whereas measurement or scale effects can normally not be included. Also scale effects may be responsible for discrepancies between physical and numerical model results if, for example, some terms such as kinematic viscosity are neglected in the numerical approach.

This article reviews exclusively scale effects and, if not particularly mentioned, for hydraulic flow phenomena and fluids interacting with non-cohesive sediments or structures, thereby extending and updating Heller (2007). Scale effects are illustrated in Fig. 1 showing the overflow spillway of Gebidem Dam and its investigation in a physical hydraulic model at scale 1 : 30. The air entrainment differs considerably despite similar flow conditions.

Generally speaking, scale effects for a specific phenomenon increase with the scale ratio or scale factor (Novak and Cabelka 1981, Hughes 1993)

$$\lambda = \frac{L_P}{L_M} \tag{1}$$

where L_P is a characteristic length in the real-world prototype (subscript P) and L_M the corresponding length in the model

Revision received 5 April 2011/Open for discussion until 31 December 2011.

ISSN 0022-1686 print/ISSN 1814-2079 online
http://www.informaworld.com

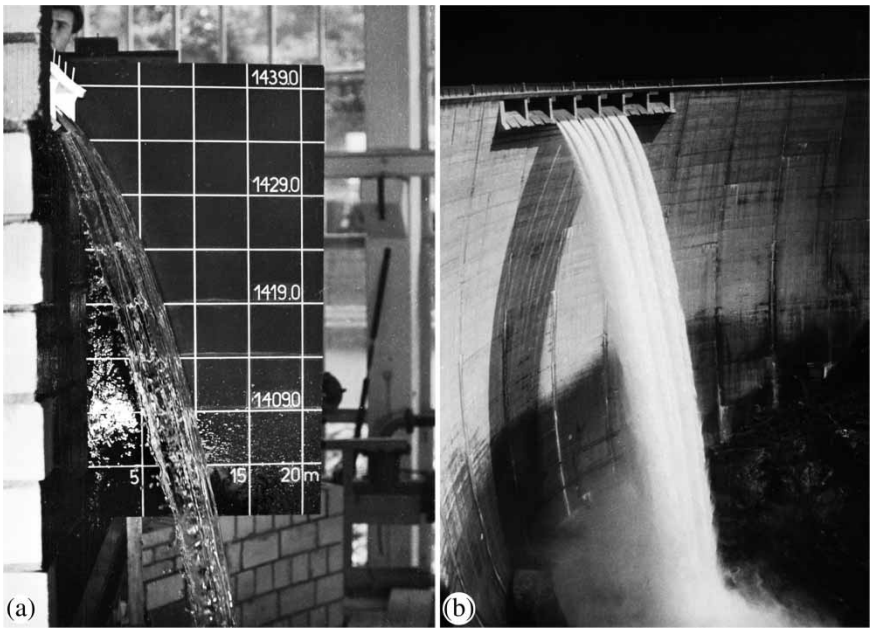

Figure 1 Overflow spillway of Gebidem Dam, Valais, Switzerland: (a) physical hydraulic model at scale 1 : 30 (VAW Foto 03-21-20), (b) real-world prototype in 1967 (VAW Dia 8870). Note that air entrainment of free jet differs considerably between model and prototype due to non-identical Weber numbers

(subscript *M*). The inverse of Eq. (1) is herein defined as the scale $1 : \lambda$. The required space, time and cost to conduct experiments increase with about λ^{-2}, $\lambda^{-1/2}$ and λ^{-3}, respectively (Le Méhauté 1976). However, with decreasing model size increasing scale effects are expected and the up-scaled model results may deviate from real-world prototype observations. The appropriate selection of λ is therefore an economic and technical optimization and λ may intentionally be selected in a range where scale effects cannot fully be neglected.

This article reviews the scattered information on scale effects concerning physical hydraulic models and aims to provide the reader with the necessary tools to judge under which conditions scale effects can be neglected in typical hydraulic flow phenomena. Model–prototype similarities including mechanical, Froude and Reynolds similarities are discussed in Section 2. Scale effects and their consequences are addressed in Section 3 and approaches to obtain model–prototype similitude and to establish limiting criteria including an example are presented in Section 4. A discussion on how significant scale effects are avoided, compensated or corrected follows in Section 5. Future research directions are proposed in Section 6, and the results are summarized in Section 7.

2 Similarities

2.1 *Mechanical similarity*

A physical scale model is completely similar to its real-world prototype and involves no scale effects if it satisfies mechanical similarity implying the following three criteria (Yalin 1971, Kobus 1980, Novak 1984, Hughes 1993, Martin and Pohl 2000, Heller 2007):

- geometric similarity;
- kinematic similarity;
- dynamic similarity.

Geometric similarity requires similarity in shape, i.e. all length dimensions in the model are λ times shorter than of its real-world prototype. Model lengths, areas and volumes therefore scale with λ, λ^2 and λ^3, respectively, in relation to the prototype. *Kinematic* similarity implies geometric similarity and in addition indicates a similarity of motion between model and prototype particles. It requires constant ratios of time, velocity, acceleration and discharge in the model and its prototype at all times. *Dynamic* similarity requires in addition to geometric and kinematic similarities that all force ratios in the two systems are identical. In fluid dynamics, the most relevant forces are (Hughes 1993):

$$\text{Inertial force} = \text{mass} \times \text{acceleration} = (\rho L^3)\left(\frac{V^2}{L}\right) = \rho L^2 V^2 \tag{2}$$

$$\text{Gravitational force} = \text{mass} \times \text{gravitational acceleration} = \rho L^3 g \tag{3}$$

$$\text{Viscous force} = \text{dynamic viscosity} \times (\text{velocity/distance}) \times \text{area} = \mu\left(\frac{V}{L}\right)L^2 = \mu VL \tag{4}$$

$$\text{Surface tension force} = \text{unit surface tension} \times \text{length} = \sigma L \tag{5}$$

$$\text{Elastic compression force} = \text{Young's modulus} \times \text{area} = EL^2 \tag{6}$$

$$\text{Pressure force} = \text{unit pressure} \times \text{area} = pL^2 \tag{7}$$

The parameters in Eqs. (2)–(7) are fluid density ρ, characteristic length L, characteristic velocity V, gravitational acceleration g, dynamic viscosity μ, surface tension σ, Young's modulus E and pressure p. Since hydraulic models are addressed, fluid parameters without subscript denote the fluid water. Any parameter for L and V can be selected, as long as they are characteristic of the investigated phenomenon. Typical parameters for L are water depth, wave height or diameter of a structure and for V approach flow velocity or wave celerity.

Dynamic similarity requires constant ratios of all forces, namely $(\text{inertial force})_P/(\text{inertial force})_M = (\text{gravitational force})_P/(\text{gravitational force})_M = \cdots = \text{constant}$. A direct consequence is that the corresponding ratios among the various forces in Eqs. (2)–(7) must be identical in the model and real-world prototype (Kobus 1980). The inertial force is normally the most relevant in fluid dynamics and is therefore included in all common force ratio combinations:

$$\text{Froude number } \mathsf{F} = \left(\text{inertial force/gravity force}\right)^{1/2} = \frac{V}{(gL)^{1/2}} \tag{8}$$

$$\text{Reynolds number } \mathsf{R} = \text{inertial force/viscous force} = \frac{LV}{\nu} \tag{9}$$

$$\text{Weber number } \mathsf{W} = \text{inertial force/surface tension force} = \frac{\rho V^2 L}{\sigma} \tag{10}$$

$$\text{Cauchy number } \mathsf{C} = \text{inertial force/elastic force} = \frac{\rho V^2}{E} \tag{11}$$

$$\text{Euler number } \mathsf{E} = \text{pressure force/inertial force} = \frac{p}{\rho V^2} \tag{12}$$

In Eq. (9), the kinematic viscosity $\nu = \mu/\rho$ was used instead of the dynamic viscosity μ.

A large number of force ratios were defined, for example, by Ettema *et al.* (2000); to reach mechanical similarity all of them have to be considered. Exact model similarity would consequently require a model operating in a *miniature universe* where all physical parameters are scaled including geometry, e.g. L, fluid properties, e.g. E, V, ρ, ν, σ, characteristics of the structure (subscript *st*), e.g. E_{st}, and also g and the atmospheric pressure. The correct modelling of the two force ratios F in Eq. (8) and R in Eq. (9) is already challenging since a constant ratio $\mathsf{R}_M/\mathsf{F}_M = \mathsf{R}_P/\mathsf{F}_P$ is required resulting in

$$\frac{g_M^{1/2}}{\nu_M} = \lambda^{3/2}\frac{g_P^{1/2}}{\nu_P} \tag{13}$$

Since the term on the right-hand side of Eq. (13) is large, this would require either model tests in a centrifuge to increase g_M and/or a fluid of very small kinematic viscosity ν_M (Kobus 1980). If the model fluid is identical as in the real-world prototype, only one force ratio can be identical between model and its prototype if $\lambda \neq 1$ and dynamic (and mechanic) similarity is impossible, therefore (Le Méhauté 1976, Kobus 1980, Hughes 1993, Martin and Pohl 2000, Heller 2007). The most relevant force ratio is therefore selected and scale effects due to the others have to be negligible.

2.2 *Froude similarity*

The criterion $\mathsf{F}_M = \mathsf{F}_P$ is most often applied in open-channel hydraulics. Froude similarity is especially suited for models where friction effects are negligible (e.g. deep-water wave propagation) or for short, highly turbulent phenomena (e.g. hydraulic jump) since the energy dissipation of the latter depends mainly on the turbulent shear stress terms. These are statistically correctly scaled in a Froude model even though the turbulent fine structures and the average velocity distribution differ between the model and prototype flows (Le Méhauté 1976, 1990, Hughes 1993). The gravitational acceleration g in Eq. (8) is not scaled, a fact which may result in scale effects for an otherwise exact Froude model. Under Froude similarity, the remaining force ratios in Eqs. (9)–(12) cannot be identical between the model and real-world prototype and may therefore result in non-negligible scale effects. The most important scaling ratios to up-scale results of a Froude model to its prototype are described by Hughes (1993) or Martin and Pohl (2000).

2.3 *Reynolds similarity*

Considering air models, laminar boundary layer problems or intake structures (Westrich, in Kobus 1980), the viscous force may be dominant and the Reynolds similarity therefore applies as $\mathsf{R}_M = \mathsf{R}_P$. Scale effects in such models result from the incorrect modelling of the remaining force ratios F, W, C and E. A serious disadvantage of the Reynolds similarity is its inconvenient scaling ratios such as λ^{-1} for velocity (Hughes 1993). A phenomenon with a velocity of 1 m/s in a real-world prototype has to be modelled with a model velocity $(1/\lambda^{-1})1 = 25{\cdot}1 = 25$ m/s at scale 1 : 25. One possibility to deal with such large

velocities is to conduct the experiment in a wind tunnel and use air instead of water (Section 5.1).

3 Scale effects

3.1 *General*

Scale effects result in deviations between up-scaled model measurements and real-world prototype observations due to prototype parameters which are not correctly scaled to the miniature universe resulting in force ratios which are not identical between the model and its prototype. The following four items are relevant, independent of the investigated phenomenon:

(1) Physical hydraulic model tests always involve scale effects if $\lambda \neq 1$ since it is impossible to correctly model all force ratios in Eqs. (8)–(12). The relevant question is whether or not scale effects can be neglected.

(2) The larger the scale ratio λ, the more the incorrect modelled force ratios deviate from the prototype ratios and the larger are the expected scale effects. However, even though scale effects increase with λ in a specific study, a given value of λ does not indicate whether or not scale effects can be neglected. Figure 2(b) shows a landslide generated impulse wave experiment with significant scale effects relative to air entrainment when compared with Fig. 2(a) even though the scale factor between Fig. 2(b) and (a) is only $\lambda = 2$. In contrast, rather small-scale effects are expected if, for example, the discharge in a 10 m wide river is investigated in a model with $\lambda = 2$. Using only λ as the limiting criterion to avoid significant scale effects is insufficient, therefore.

(3) The size of scale effects depends on the investigated phenomenon or parameter in a given model study since the relative importance of the involved forces may differ. If one parameter, such as discharge in Fig. 1, is not considerably affected by scale effects, it does not necessarily mean that other parameters, such as the jet air concentration, are also not affected. Each involved parameter requires its own judgement regarding scale effects.

(4) Since fluid forces in a model are more dominant than in the real-world prototype, scale effects normally have a 'damping' effect. Parameters such as the relative wave height (Fig. 2), the relative discharge or the transported relative volume of sand (Ranieri 2007) are normally smaller in the model than in its prototype. A judgement if the prediction based on the model under- or over-estimates the prototype value is therefore often possible.

3.2 *Specific items*

The *Froude number* is nearly always identical between model and prototype in hydraulic modelling (Section 2.2) and few details on scale effects due to incorrectly considered F are available. The Froude number may result in non-negligible scale effects if Reynolds similarity is applied. The effect of the gravity force on fluid flow should therefore be negligible in a Reynolds model (Westrich, in Kobus 1980).

The *Reynolds number* is relevant for seepage flows, creeping flows around spheres or particularly at boundaries resulting in excessive losses in a model compared with its real-world prototype. One example is the normally faster wave decay in a model. Since most flows at real-world scale are both turbulent and in the hydraulic rough regime, where losses are independent of R (e.g. Moody-diagram), flows in hydraulic Froude models are often 'shifted' to the hydraulic rough regime to better account for losses (Section 5.2).

No model with *Weber similarity* was ever built according to Le Méhauté (1976) and W may therefore always be a source of scale effects. The fountain shown in Fig. 3 is a rare case

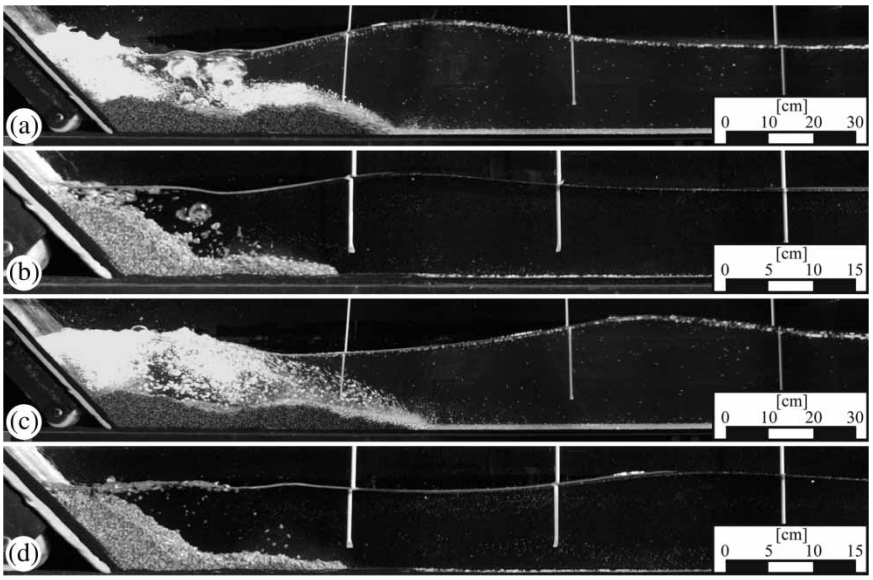

Figure 2 Impulse waves scale series: different air entrainment and detrainment of two scale models with $\mathsf{F}_I = V_s/(gh)^{1/2} = 2.5$ at similar relative time $t(g/h)^{1/2}$ between (a,b) and (c,d) with (a,c) $\mathsf{R}_I = 289{,}329$, $\mathsf{W}_I = 5345$ and (b,d) $\mathsf{R}_I = 103{,}415$, $\mathsf{W}_I = 1336$ (Heller *et al.* 2008)

Figure 3 Surface tension effects in water fountain at Rämistrasse, Zurich, resulting in separation of water sheet (Photo V. Heller)

where surface tension is relevant in a real-world prototype of such a large dimension, resulting in the separation of the thin water sheet. Surface tension is negligible for most prototypes in hydraulic engineering; however, it is relevant in scale models for air entrainment (wave breaking), small water depths, small waves (capillary waves) or large fluid curvatures (Martin and Pohl 2000). A dominant surface tension in the model may cause larger relative air bubble sizes and faster air detrainment, resulting in smaller volume fractions of air (Chanson 1996). Since the air bubble size is not correctly scalable, phenomena including air flow have to be modelled at a relatively large scale to avoid significant scale effects (Chanson 2009). Air entrainment may also be a function of the atmospheric pressure (in dimensionless form an Euler number), which would have to be scaled to the miniature universe for exact modelling.

The *Cauchy number* considers compression via Young's modulus E. Since E of water is not scaled, water may behave too hard in the model for impact phenomena. Compressibility is also relevant for shock waves due to underwater explosions (Le Méhauté 1990) or in pipes (Joukovski shock). For most other phenomena, water compressibility may be neglected. However, the Cauchy number is relevant for fluid–structure interactions. Young's modulus E_{st} of a distensible structure has to be scaled to the model scale without changing the Poisson number (Le Méhauté 1976). In a Froude model, E_{st} scales linearly with λ. An identical model material as in the prototype results in a λ-times too stiff model structure. Such an incorrect structural scaling was partly responsible for the Sines breakwater failure (Oumeraci 1984, Le Méhauté 1990). The parameter E is further relevant if air instead of water is employed (Section 5.1), for air–water mixtures or for studies involving ice (Michel 1970, cited Kobus 1980). The physical modelling of mooring lines or fenders is challenging. Instead of scaling fenders including E_{st}, they are sometimes modelled with a spring system to include the non-linear behaviour.

The *Euler number* considers pressure force relevant for high pressures in pipes or cavitation of turbines, pumps or hydraulic structures. The cavitation number $\mathrm{Ka} = (p_0 - p_v)/(\rho V_0^2/2)$, describing the tendency, stage and severity of cavitation (Naudascher, in Kobus 1980), is the difference of two Euler numbers including the absolute static pressure p_0, velocity V_0 at a specific location and vapour pressure p_v. Scale effects due to an incorrectly modelled Ka in a Froude model would exclude the observation of cavitation. However, cavitation occurs if the model tests take place in a cavitation tunnel where p_v is scaled to the miniature universe. Even then the investigation of cavitation is challenging since it depends on parameters including the number of nuclei, physical water properties such as temperature or gas content or the hydrodynamic flow characteristics such as turbulence (Keller, in Kobus 1980).

4 Approaches for model–prototype similitude

4.1 *Inspectional analysis*

Inspectional analysis operates with the set of equations describing the hydrodynamic force balances. This includes any type of equation that mathematically translates a physical phenomenon, e.g. the Reynolds-averaged Navier–Stokes equation. Similarity requires that both the model and real-world prototype follow the identical set of equations. The ratios of the corresponding terms in the model and prototype equations result in similarity criteria as shown in Eqs. (8)–(12). This method can only be applied if the physics of a phenomenon is such that the relevant equations can be formulated. Inspectional analysis allows a quantification of the relative importance of all involved terms and the definition of a minimum scale where significant scale effects are avoided. Inspectional analysis also adds to the understanding of a phenomenon (Le Méhauté 1990).

4.2 *Dimensional analysis*

Dimensional analysis is a most useful tool in experimental fluid mechanics, allowing for the implicit formulation of criteria for dynamic similarity in a simple and direct manner (Kobus 1980). It is based on the Π-theorem of Buckingham (1914), as described by, for example, Raghunath (1967), Yalin (1971), Novak and Cabelka (1981), Spurk (1992) or Hughes (1993). A physical problem with n independent parameters $q_1, q_2, \ldots, q_n$ can be reduced to a product of $n - r$ independent, dimensionless parameters $\Pi_1, \Pi_2, \ldots, \Pi_{n-r}$ with r as the minimum

number of reference dimensions (length [L], mass [M] or time [T]) required to describe the dimensions of these n parameters. Similarity requires that each of these dimensionless parameters quantitatively agree between model and real-world prototype. The dimensionless parameters include the geometrical ratios as well as the force ratios F, R, W, C and E in Eqs. (8)–(12).

These dimensionless parameters allow for a general presentation of results and since they are related as a function of dimensionless parameters, no scale ratios are required to up-scale them. The number of necessary tests is normally reduced since the number of physical parameters characterizing the phenomenon is reduced from n to $n - r$. However, in contrast to inspectional analysis, the relative importance of the dimensionless parameters on the phenomenon remains unknown. The dimensional analysis results in an arbitrariness in determining the conditions of similitude if the phenomenon includes more than six parameters n and it is strongly criticized, for example, by Le Méhauté (1990). Nevertheless, it is widely applied in hydraulic modelling. It is recommended using dimensional analysis only if the level of theoretical understanding of a phenomenon allows no inspectional analysis.

4.3 *Calibration*

Model–prototype similarity can be achieved if tests in the physical model are conducted for configurations where real-world prototype data are available. If the relative parameters agree well between model and prototype and significant model and measurement effects can be ruled out, negligible scale effects are expected and model–prototype similarity is reached. This gives confidence that model results of other test configurations can also be applied to the prototype without large deviations. A prerequisite for this method is reliable prototype data. Observed model–prototype deviations despite kinematic similarity may help to quantify scale effects and to correct them in other test configurations or it can at least be stated in which way (over- or under-estimation) scale effects affect the results.

4.4 *Scale series*

In a scale series, at least three kinematic similar models of different λ are employed and similar tests conducted in all models scaled with the appropriate scale ratios are compared. The largest model acts as a reference and is quasi-replacing the real-world prototype in calibration (Section 4.3). Deviations of the dimensionless results of the smaller compared with the largest model are due to scale effects. This method allows scale effects to be quantified or at least to indicate in which way scale effects change the results and the definition of limiting criteria is possible. Disadvantages are the large experimental effort compared with the other three methods and the uncertainty of whether or not the largest model itself is already affected by non-negligible scale effects.

4.5 *Example: landslide generated impulse waves*

This example shows both how Froude model similitude is obtained and how significant scale effects are avoided. Impulse waves were investigated in an 11 m long, 0.5 m wide and 1 m deep wave channel. The granular slide material was pneumatically accelerated and the resulting impulse wave features were measured with capacitance wave gauges (Heller and Hager 2010).

To obtain model similarity, a combination of some of the above approaches was applied. The Cauchy number was not considered since the fluid was practically incompressible and the effect of the Euler number was neglected because of the free-surface nature of the phenomenon. Scale effects in this Froude model were therefore mainly expected from the Reynolds and Weber numbers. Inspectional analysis was not applied since the analytical understanding of this three-phase phenomenon was insufficient.

Dimensional analysis

Figure 4 shows a definition sketch of impulse wave generation with the main parameters affecting the impulse wave features. Seven governing parameters were independently varied, namely the still water depth h [L], slide (subscript s) impact velocity V_s [LT^{-1}], slide thickness s [L], bulk slide volume $\forall_s$ [L^3], bulk slide density ρ_s [ML^{-3}], grain (subscript g) diameter d_g [L] and the slide impact angle α [°]. Besides these, the water density ρ [ML^{-3}], gravitational acceleration g [LT^{-2}], horizontal distance x [L] from the coordinate origin and time t [T] also have an effect on the unknown wave features, including the water-surface displacement η or the maximum wave amplitude a_M (Heller *et al.* 2008). The z coordinate and the slide mass m_s were not considered as the latter is represented by the product $\rho_s \forall_s$. The selected $n = 11$ independent parameters include $r = 3$ reference dimensions (length [L], mass [M] and time [T]) resulting in $n - r = 11 - 3 = 8$ dimensionless parameters. The r selected reference parameters are h, g and ρ. The eight dimensionless parameters Π_1, Π_2, …, Π_8 were found with a balance of the reference dimensions. The unknown exponents β, γ and δ were computed, for example, for V_s as

$$\Pi_1 = V_s h^\beta g^\gamma \rho^\delta \text{ or} \tag{14}$$

$$[-] = [LT^{-1}][L]^\beta [LT^{-2}]^\gamma [ML^{-3}]^\delta \tag{15}$$

Equation (15) applied to each reference dimension gives

$$\begin{array}{lrcl} [L]: & 0 & = & +1+1\beta+1\gamma-3\delta \\ [T]: & 0 & = & -1+0\beta-2\gamma+0\delta \\ [M]: & 0 & = & +0+0\beta+0\gamma+1\delta. \end{array} \tag{16}$$

The solution of Eq. (16) is $\beta = -1/2$, $\gamma = -1/2$ and $\delta = 0$ and Eq. (14) results in $\Pi_1 = V_s/(gh)^{1/2}$, i.e. the slide Froude number F_I in impulse (subscript I) waves. The remaining Π parameters are relative slide thickness $\Pi_2 = s/h$, relative

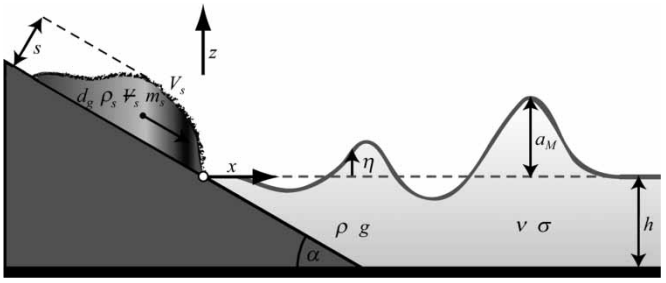

Figure 4 Definition sketch of impulse wave generation (after Heller *et al.* 2008)

bulk slide volume $\Pi_3 = \forall_s/(bh^2)$, $(\forall_s/h^3)$ multiplied by (h/b) to include channel width b, relative slide density $\Pi_4 = \rho_s/\rho$, relative distance $\Pi_5 = x/h$, relative grain diameter $\Pi_6 = d_g/h$, relative time $\Pi_7 = t(g/h)^{1/2}$ and slide impact angle $\Pi_8 = \alpha$. A consideration of kinematic viscosity ν and surface tension σ in the dimensional analysis would result in an impulse Reynolds number $\mathsf{R}_I = g^{1/2}h^{3/2}/\nu$ and Weber number $\mathsf{W}_I = \rho g h^2/\sigma$. To obtain model–prototype similitude for a specific run, each of these eight dimensionless parameters Π_1, Π_2, …, Π_8 requires an identical value in the model and its real-world prototype.

Calibration

The effects of impulse waves are often visible immediately after an event at the shore line vegetation. The 1958 landslide generated impulse wave at Lituya Bay, Alaska, destroyed the forest at the opposite shore up to a maximum run-up height of 524 m. This run-up height was satisfactorily modelled by Fritz *et al.* (2001) with the present impulse wave set-up at a scale of 1 : 675, a water depth of $h = 0.18$ m, $\mathsf{R}_I \approx 240{,}000$ and $\mathsf{W}_I \approx 4350$.

Scale series

Scale effects were quantified with seven scale series by Heller *et al.* (2008). All seven governing and further geometric parameters were scaled following the Froude scale ratios, such as the spacing between the wave gauges which were reduced from 1.00 m to 0.50 m at a scale ratio $\lambda = 2$ and to 0.25 m at $\lambda = 4$, to assure that each of the dimensionless parameters remained constant within a scale series. The goal of the investigation was to define limiting Reynolds and Weber numbers for which scale effects relative to the maximum wave amplitude a_M can be neglected (Fig. 4). Figure 5 shows the relative water surface displacement η/h versus relative time $t(g/h)^{1/2}$ at different relative distances x/h of scale series S4. The reference test was S4/1 with a still water depth of $h = 0.400$ m, S4/2 was scaled with $\lambda = 2$ resulting in $h = 0.200$ m and S4/3 with $\lambda = 4$ resulting in $h = 0.100$ m. The profile of the relevant primary wave of S4/2 follows the reference test S4/1, whereas the profile of S4/3 is smaller due to scale effects. Scale effects for impulse wave generation are further illustrated in Fig. 2

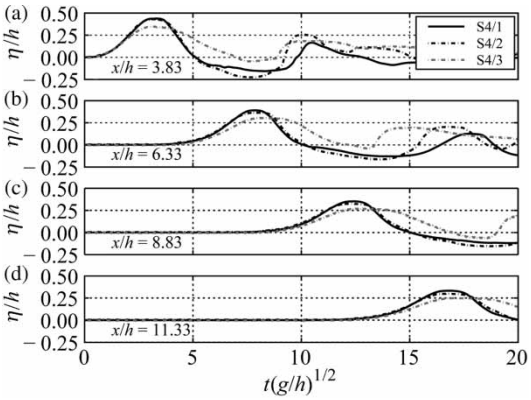

Figure 5 Impulse waves scale series tests: normalized water surface displacement η/h versus relative time $t(g/h)^{1/2}$ at three different scales of runs S4/1 with $h = 0.400$ m, S4/2 with $h = 0.200$ m and S4/3 with $h = 0.100$ m (Heller *et al.* 2008)

showing photos of two runs with $h = 0.200$ m and $h = 0.100$ m, respectively, at similar relative time between Fig. 2(a,b), and Fig. 2(c,d). Figure 2(b,d) is increased by a factor 2. Considerable differences in air entrainment and detrainment are observed between Fig. 2(a,b) and Fig. 2(c,d), respectively, mainly due to different W. Considering all seven scale series, scale effects are negligibly small (<2%) relative to the maximum wave amplitude a_M, if $\mathsf{R}_I = g^{1/2}h^{3/2}/\nu \geq 300{,}000$ and $\mathsf{W}_I = \rho g h^2/\sigma \geq 5000$ resulting in the rule of thumb $h \geq 0.200$ m for typical laboratory conditions (Heller *et al.* 2008).

5 Common practice to deal with scale effects

5.1 *Avoidance*

The correct way to avoid significant scale effects in a Froude model would require satisfying limiting values for the force ratios in Eqs. (8)–(12). Often rules of thumb are applied instead, without repeating the procedure described in Section 4. Table 1 shows different investigations and phenomena with rules of thumb, prototype features to which they are related to and references. These guidelines may be misleading if, for example, just a limiting scale factor λ or water depth h on its own is applied without considering to which prototype features they were defined (Section 3.1). Column 4 in Table 1 aims to consider this relevant prototype relation.

Table 2 shows typical applied scales for the investigation of different phenomena. In contrast to Table 1, the scales in Table 2 do not necessarily indicate that scale effects are negligible since they represent a compromise between both reasonable model size (economics) and moderate scale effects (Le Méhauté 1990, Hughes 1993). Since the related prototype features are unavailable, the scales in Table 2 may only be applied for 'typical' prototype dimensions and their most common flow phenomena.

Table 1 Limiting criteria to avoid significant scale effects in various hydraulic flow phenomena

Investigation	Phenomenon	Rule of thumb	Related prototype features	Reference
Air-entraining free vortex at horizontal intake	Flow conditions	$Q_i/(z_i\nu) > 30{,}000$ and $\rho Q_i^2 z_i/(A_i^2\sigma) > 10{,}000$	Scale series: largest discharge 0.009 m^3/s, largest submergence depth 0.8 m, constant intake diameter = 0.0762 m	Anwar *el al.* (1978)
Broad-crested weir	Discharge coefficient	Overfall height ≥ 0.07 m	Weir length 0.15 – 5 m, weir width 4.88 m	Hager (1994)
Dam break wave	Sudden failure, dam in smooth rectangular channel	Still water depth ≥ 0.30 m	n.a.	Lauber and Hager (1998)
Dam with ski jump	Lateral overfall weir, spillway capacity, ski jump, flow conditions in stilling basin	Scale 1 : 30	Upper Siebertalsperre, dam height 90 m, $Q_d = 140\ m^3/s$	Bretschneider, in Kobus (1980)
Dike breaching	Hydraulics over dike consisting of uniform and non-cohesive material	Unit discharge ≥ 20 1/s and $d_g \geq$ 1 mm	Scale series: largest scale with dike height = width = 0.40 m and d_g= 8 mm	Schmocker and Hager (2009)
Hydraulic jump	Sequent depths ratio h_2/h_1	$V_1h_1/\nu > 100{,}000$ for $F_1 < 10$ and $h_1/b < 0.1$	Scale series: maximum $h_1 = 0.063$ m, maximum $F_1 = 42.7$	Hager and Bremen (1989)
Hydraulic jump	Void fraction and bubble count rate distributions, bubble chord time	$\rho V_1 h_1/\mu > 100{,}000$	Scale series: maximum $h_1 = 0.024$ m, maximum b =0.50 m, maximum $F_1 = 8.5$	Chanson (2009)
Impulse wave	Generation by subaerial landslide	$R_I \geq 300{,}000$ and $W_I \geq 5000$ resulting in $h \geq 0.200$ m	Scale series: maximum $h = 0.60$ m, $1.7 \geq V_s/(gh)^{1/2} \leq 4.3$	Heller *et al.* (2008)
Mountain river	Bed morphology	Scale 1 : 10 to 1 : 20	Steinibach, $d_m = 0.20$ m, $d_{90} = 0.52$ m, $d_{max} = 0.90$ m, slope 3 – 13%	Weichert (2006)
River expansion	Bed load transport	Scale 1 : 55, d_g >0.22 mm and correction grain size distribution	$d_m = 0.043$ m, $d_{90} = 0.096$ m	Zarn (1992)
Rubble mound breakwater	Stability	Limiting scale as a function of prototype wave height in Fig. 1 of Oumeraci (1984)	Prototype wave height up to 13 m	Oumeraci (1984)
Scour	Bridge pier and abutment scour depth development prediction with Eq. (1) of Oliveto and Hager (2005)	0.60 < threshold Froude number < 1.20, width pier/$b \geq 0.05$, width abutment/$b \geq$0.05	Model tests: width pier = 0.022 – 0.500 m, width abutment = 0.05 – 0.20 m, $0.45 \leq t \leq 21.0$ days, $b = 1.0$ m, $0.03 \leq h \leq 0.18$ m, $d_{50} \geq 0.80$ mm, $1.07 \leq V/(g'd_{50})^{1/2} < 4.26$ with $g' = [(\rho_s - \rho)/\rho]g$	Oliveto and Hager (2005)
Scour	Effect of large-scale turbulence on equilibrium scour depth at cylinders	Cylinder diameter > 0.400 m for scale effect ≤ 5%	Model tests: cylinder diameter = 0.064 – 0.406 m, average velocity = 0.46 m/s, $v^*/v^*_c = 0.80$, $d_m = 1.05$ mm, h =1.000 m	Ettema *et al.* (2006)
Sharp-crested weir	Lower nappe profile	Overfall height ≥ 0.045 m	Scale series: maximum overfall height = 0.045 m	Ghetti and D'Alpaos (1977)
Ski jump	Jet throw distance	Approach flow depth ≥ 0.04 m	Scale series: largest water depth 0.07 m	Heller *et al.* (2005)
Skimming flow on stepped spillway	Turbulence level, entrained bubble sizes and interfacial areas	$\rho(gh_c^3)^{1/2}/\mu > 500{,}000$ and step height > 0.02 m	Scale series: maximum step height 0.143 m, spillway slopes 3.4 – 50°	Chanson (2009)
Spillway	Amount of air entrainment from aerator	$V/[\sigma/(\rho h)]^{1/2} > 110$	Measurements in models and a small prototype and consideration of further prototype data	Rutschmann (1988)
Stepped spillway	Flow velocity profile air–water mixture	Scale ≥ 1 : 15	Step height 0.6 m, maximum specific discharge 20 m^2/s	Boes (2000)
Surf zone beach profile	Volume of transported sand	Scale ≥ 1 : 7.5, $d_{50} = 0.13$ mm, significant wave height 0.20 m, peak wave period 2.0 s	$d_{50} = 0.335$ mm, significant wave height 1.5 m, peak wave period 6.0 s	Ranieri (2007)
Vertical plunging circular jet	Void fraction and bubble count rate distributions, bubble size	$\rho V_j^2 d_j/\sigma > 1000$	Scale series: largest jet diameter 0.025 m, jet Froude number up to 10	Chanson (2009)
Wave overtopping at coastal structures	Overtopping velocity	$2(R - R_c)^2/(\nu T) > 1000$ and $V_R^2 h_R \rho/\sigma > 10$	Theoretically deduced	Schüttrumpf and Oumeraci (2005)
Wave run-up	Run-up velocity	$2(R - R_c)^2/(\nu T) > 1000$ and $V_R^2 h_R \rho/\sigma > 10$	Theoretically deduced	Schüttrumpf and Oumeraci (2005)
Water wave	Force on slope during wave breaking	Wave height > 0.50 m	Scale series: maximum wave height 1.25 m	Skladnev and Popov (1969)
Water wave	Theoretical effect of surface tension	$T > 0.35$ s, $h > 0.02$ m	Wave with wave length where surface tension effects contribute less than 1%	Hughes (1993)

Notes: n.a.=not available; for symbols, see Notation.

Table 2 Typical model scales as compromise between reasonable size (economics) and moderate scale effects; scale effects may therefore not necessarily be negligible

Investigation	Typical scale	Reference
Beach, shoreline process	1 : 100 (vertical), 1 : 300 (horizontal)	Le Méhauté (1990)
Bottom outlet	1 : 50 to 1 : 100	Le Méhauté (1990)
Breakwater stability in short waves	1 : 30 to 1 : 50	Le Méhauté (1990), Hughes (1993)
Force on solid body in short waves	1 : 10 to 1 : 50	Hughes (1993)
Harbour penetration of short waves	1 : 50 to 1 : 150	Hughes (1993)
Hydraulic model to investigate cavitation	1 : 10 to 1 : 30	Keller, in Kobus (1980)
Intake	1 : 50 to 1 : 100	Le Méhauté (1990)
Long waves in distorted estuarine system	1 : 100 to 1 : 150 (vertical), 1 : 300 to 1 : 800 (horizontal)	Hughes (1993)
Long waves in distorted harbour or port	1 : 50 to 1 : 100 (vertical), 1 : 80 to 1 : 400 (horizontal)	Hughes (1993)
Long waves in undistorted harbour	1 : 50 to 1 : 150	Hughes (1993)
Long waves in undistorted inlet	1 : 75 to 1 : 150	Hughes (1993)
Offshore and harbour investigation (diffraction, refraction, reflection)	1 : 60 to 1 : 150	Kohlhase and Dette, in Kobus (1980)
River	1 : 100 (vertical), 1 : 800 (horizontal)	Le Méhauté (1990)
Rockfill cofferdam	1 : 30 to 1 : 50	Le Méhauté (1990)
Rubble mound breakwater stability	1 : 20 to 1 : 80	Oumeraci (1984)
Ship dynamics problem	1 : 100	Le Méhauté (1990)
Ship motion study in long waves	1 : 80 to 1 : 120	Hughes (1993)
Short wave reflection at porous breakwater	1 : 10 to 1 : 20	Oumeraci (1984)
Spillway	1 : 50 to 1 : 100	Le Méhauté (1990)
Stability study in waves (rubble mound breakwater, for input to compression study)	1 : 5 to 1 : 30	Kohlhase and Dette, in Kobus (1980)
Water power structure	1 : 50 to 1 : 100	Le Méhauté (1990)
Waves on structure (reflection, wave pressure distribution)	1 : 30 to 1 : 60	Kohlhase and Dette, in Kobus (1980)
2D wave transformation of short waves	1 : 10 to 1 : 50	Hughes (1993)
3D wave transformation of short waves	1 : 25 to 1 : 75	Hughes (1993)

Replacement of fluid

Significant scale effects due to kinematic viscosity can also be avoided if air instead of water is used in the model. Classic studies in wind tunnels were also motivated by the more advanced measurement techniques to measure turbulence in air. Disadvantages of air models are that gravity, free-surface and cavitation effects are not reproduced (Westrich, in Kobus 1980). Inertial and viscous forces are correctly modelled and it was suggested to apply Reynolds similitude for air models (Section 2.3).

Rouse *et al.* (1959) investigated the turbulence characteristics of hydraulic jumps with an air model by applying Froude similitude, thereby modelling the free surface with a rigid structure. The air compressibility is negligible if the Mach number equal to $C^{1/2}$ is <0.3 (Kundu and Cohen 2004). A maximum air flow velocity of 60 – 90 m/s reduced compressibility effects, whereas Westrich, in Kobus (1980) suggested 50 m/s for typical laboratory conditions.

Figure 6 shows an example where similar sediment morphologies occur in different fluid flows: Fig. 6(a) shows a hydraulic model of bridge pier scour using water, resulting in tailwater ripples. Similar ripples are shown in Fig. 6(b) caused by the wind on a dune. Such structures are also caused by the wind on snow surfaces. To avoid significant scale effects, both the fluid and/or the sediment are replaced (Kobus 1980), i.e. the transport of sand in water was simulated by means of coal dust in glycerin.

The fluid properties were also changed to avoid significant scale effects, such as by Ghetti and D'Alpaos (1977) or Miller (1972) who added a surfactant to the water to lower surface tension effects. Stagonas *et al.* (2010) compared test results of breaking waves both involving fresh water with $\sigma = 0.072$ N/m and a mixture of 90% distilled water and 10% isopropyl alcohol solution with $\sigma = 0.043$ N/m. They concluded that the breaker's shape and evolution, air entrainment and energy dissipation change significantly. Figure 7 compares

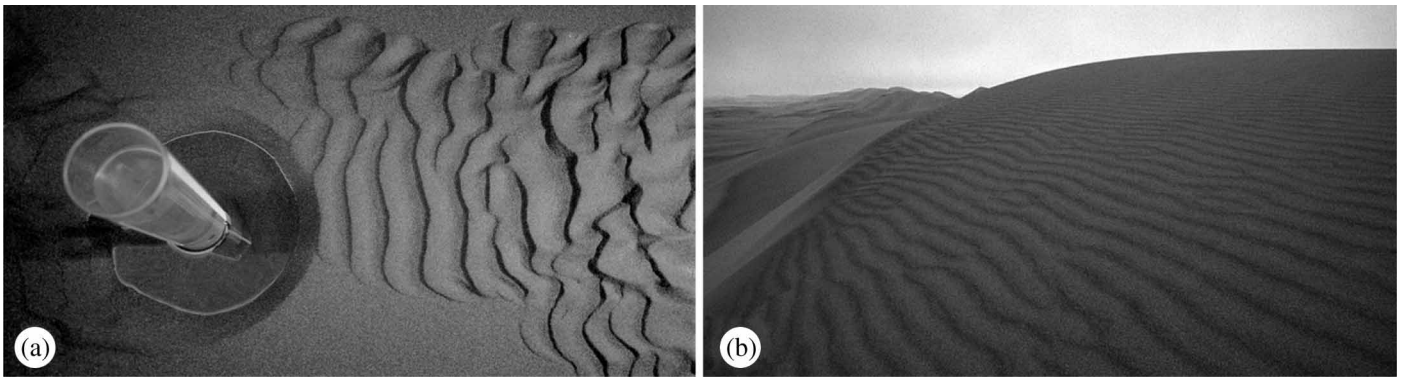

Figure 6 Replacement of fluid: similar morphologies in sand caused by fluid (a) water: ripples in hydraulic model to investigate bridge pier scours (Photo W.H. Hager), (b) air: ripples on sand dune in Swakopmund, Namibia (http://www.kapstadt.org)

air entrainment due to a vertical plunging jet in (a) fresh water and (b) an identical mixture as applied by Stagonas *et al.* (2010). Much smaller and more air bubbles are entrained in (b) than in (a). A similar effect is observed in Fig. 2 due to different scales. However, studies comparing wave breaking strongly contradict in their conclusions about how the air bubble size distribution changes in fresh and sea water (Stagonas 2010).

5.2 *Compensation*

Compensation is achieved by distorting a model geometry by giving up exact geometric similarity of some parameters in favour of an improved model–prototype similarity (Martin and Pohl 2000). Such parameters include model roughness, length scale or grain diameter in movable bed models.

Roughness

Open channel flows with a fixed bed (also including models with loose non-cohesive material if the bed form does not change) are normally modelled with Froude similarity. Non-negligible scale effects may be caused by surface tension and viscosity, mainly due to boundary roughness. The roughness coefficient increases with decreasing R in regions of the Moody diagram. Reducing the wall roughness by ignoring geometric roughness similarity can result in an identical friction coefficient in both the model and real-world prototype despite different Reynolds numbers, resulting in a compensation of scale effects. A similarity of the water surface and energy gradients is therefore achieved. This is only possible in a limited region of the Moody diagram and for a model not too small (Kobus 1980, Martin and Pohl 2000). Webb *et al.* (2010) discuss also how the roughness is properly represented in a model for a fixed bed in the hydraulic rough regime and highlight accuracies and limitations of the

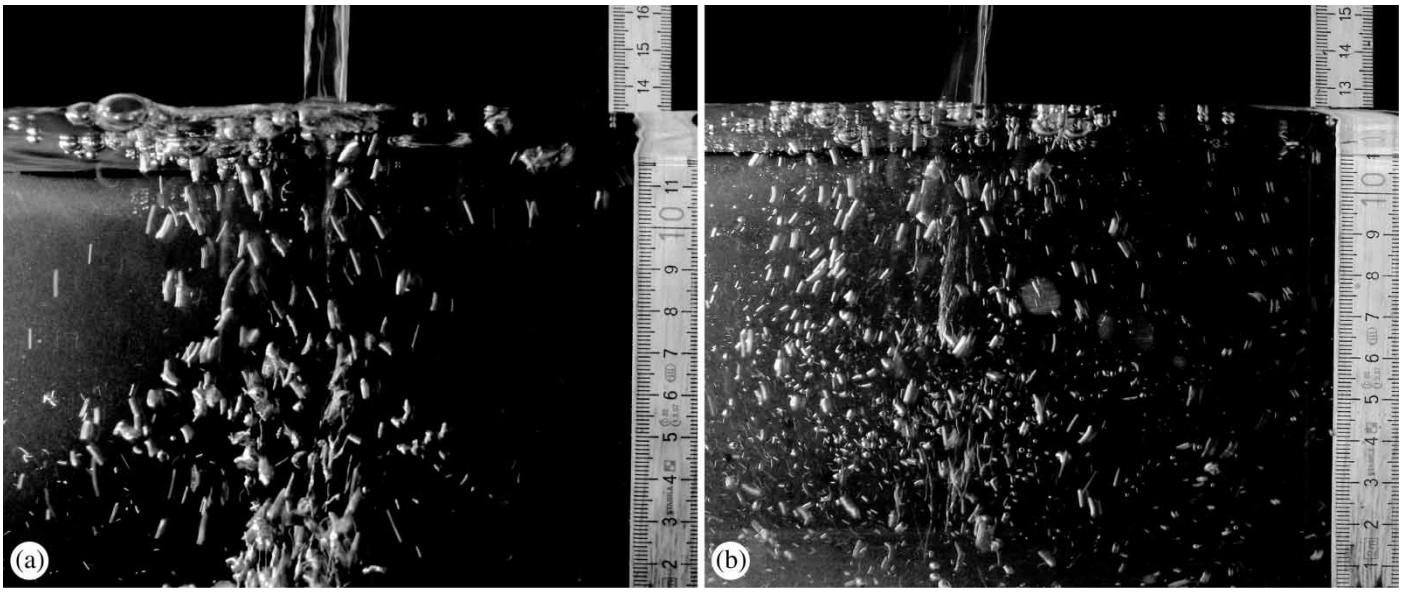

Figure 7 Replacement of fluid: air entrainment characteristics due to vertical jet impacting (a) fresh water; (b) mixture of 90% distilled water and 10% isopropyl alcohol (Photos V. Heller)

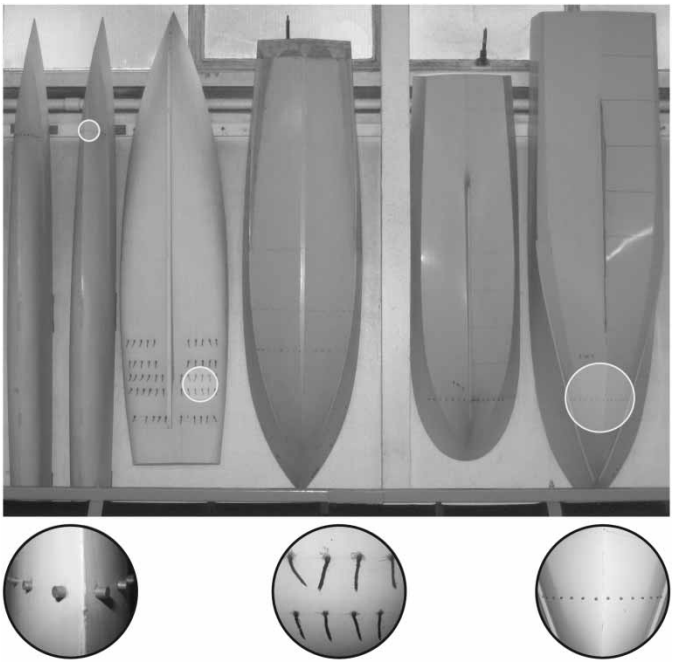

Figure 8 Model ship hulls at Solent University, Southampton, with artificial roughness structures to reach model–prototype drag force similarity (Photos V. Heller)

hydraulic roughness scaling equations based on the Manning roughness coefficient. An accurate consideration of boundary friction is further relevant for the drag force in small-scale ship models as shown in Fig. 8. They often have artificial roughness elements on the hull to 'shift' boundary layer roughness in the turbulent rough regime for an appropriate modelling of the prototype roughness (Le Méhauté 1976).

Length distortion

Model length distortion is popular in fluvial hydraulics (Knauss, in Kobus 1980, Martin and Pohl 2000). The height (subscript H) scale factor λ_H is thereby smaller than the width and length-scale factor λ. Positive effects are an increased water depth, decreased scale effects since R and W increase, higher flow velocities and a 'shift' from the hydraulic smooth to the rough flow regime. The relative measurement accuracy is improved as well and the duration of a run is reduced. Disadvantages include that 2D and 3D flow processes are incorrectly modelled and that the correct model roughness representing the real-world prototype has to be found via calibration (Knauss, in Kobus 1980, Kobus 1980, Martin and Pohl 2000).

Movable bed

Sediment transport and its initiation in movable bed models are modelled with Froude similarity using the grain Froude number $\mathsf{F}^{*2} = \rho/(\rho_s - \rho)v^{*2}/(gd_g)$, with the shear velocity $v^* = (ghS_E)^{1/2}$ and energy line slope S_E. The motion of suspended material and its initiation depend not only on F^* but also on the grain Reynolds number $\mathsf{R}^* = v^* d_g/\nu$ (Shields diagram) and the free surface is a function of bed roughness. Further relevant are the grain density and the grain diameter which cannot follow any scale without being affected by cohesion or changing from bed load transport in the prototype to suspended load transport in the model (Kamphuis 1974). This results in various similarity criteria which have to be satisfied simultaneously in a movable bed model (Kamphuis 1974, Oumeraci 1984). Normally, those criteria are only fulfiled, if at all, in a length-distorted model. Sometimes the sediment density is reduced and a larger grain diameter is employed to reach the same flow–sediment interaction behaviour. The time scale is unknown and has to be evaluated with a 'historical' test case from real-world data. A calibration of the model with high-quality real-world data is therefore essential (Gehrig, in Kobus 1980).

The scale limitation of the grain diameter d_g in sediment transport modelling is discussed by Zarn (1992). The diameter d_g can often not be scaled with the same scale factor λ as the model main dimensions since it may result in $d_g < 0.22$ mm for which the flow–grain interaction characteristics changes, affecting, e.g. sediment transport. Zarn (1992) proposes a method to modify the model grain size distribution accordingly. Bretschneider, in Kobus (1980), suggests that the grain diameter at 50 wt% d_{50} should be >0.5 mm to rule out cohesion effects, in agreement with Oliveto and Hager (2005) working with limiting $d_{50} = 0.80$ mm and Schmocker and Hager (2009) using a limiting grain diameter of $d_g = 1$ mm.

5.3 *Correction*

Economic considerations, limited space or time may be reasons to intentionally build a small model where non-negligible scale effects are expected (Stagonas 2010). An extreme case is the *classical* micro-model, a small river model with λ_H of up to 20,000 suggested for demonstration, education and communication purposes (Maynord 2006). Except for these extreme cases where the model–prototype results may deviate too much, the model results may afterwards be corrected for phenomena where enough information on the quantitative influence of scale effects is available. For example, solitary waves decay normally faster in the model than in the prototype due to boundary layer effects and fluid viscosity. Keulegan (1950) presents analytical equations to compute and correct for both effects. Oumeraci (1984) includes correction coefficients for the stability of rubble mound breakwater model investigations. Ettema *et al.* (2006) provide means to reduce equilibrium scour-depth estimates obtained from small-scale cylinders in experiments accounting for the incorrectly modelled large-scale turbulence if the bed-sediment entrainment similitude criterion is applied. Ranieri (2007) deduces distortion coefficients to correct the slopes of movable surf zone beach profiles under wave action a posteriori since coastal sediment transport is incorrectly modelled in small Froude models. Cuomo *et al.* (2010) present a method on how wave

impact pressures from small-scale models can be up-scaled with Froude scale ratios and correction factors taking air leakage in the impact zone into account.

6 Future research directions

The basics of similitude theory have been known for a long time. Modern laboratory techniques and instrumentation allow for the investigation of scale series of complex phenomena, even if several dynamic parameters are involved. The quality of field data is further increased due to both more sophisticated field measurement systems and methods, and increasing effort in field campaigns. More reliable calibrations may be possible in future.

Future research may include combinations of already established methods: what is the role of an un-scaled atmospheric pressure on air entrainment? The answer may be found with fluids of reduced surface tension employed in a cavitation tunnel. How would the scaling of g affect the model results? The scaling of g is already common in geotechnics where phenomena such as landslides or foundations are modelled in centrifuges (Taylor 1995). There exists, to the author's knowledge, no study where all relevant parameters were scaled to the miniature universe, such as g and the atmospheric pressure simultaneously. This may be possible, e.g. employ a cavitation tunnel on a continuous accelerating platform.

Numerical simulations may serve as a more frequently used alternative for the investigation of phenomena such as turbidity currents or distensible structures, which may not be addressed in physical models without significant scale effects or simulations may even play a role in the quantification of scale effects as shown by Huang *et al.* (2009) for turbulent flows and bridge pier scour. A Direct Numerical Simulation includes the full Navier–Stokes equations and therefore also, for example, the kinematic viscosity responsible for scale effects in a Froude model. Numerical simulations of a scale series may reveal the isolated effect of such terms on a phenomenon even if it is only qualitatively modelled. Such simulations would also have the advantage that the measurement error is not increasing with decreasing scale as is common in physical hydraulic model studies. It may even be useful to scale all relevant parameters numerically to the miniature universe in future.

7 Conclusions

This article reviews scale effects in hydraulic engineering, describes and illustrates their effects in different phenomena, addresses how to avoid significant scale effects and provides the relevant bibliography for typical hydraulic flow phenomena. The most relevant issues are summarized as follows.

- The basics of the similarity theory between physical hydraulic models and real-world prototypes were reviewed including mechanical, Froude and Reynolds similarity. The most relevant force ratios to obtain dynamic similarity include the Froude, Reynolds, Weber, Cauchy and Euler numbers.
- A model with $\lambda \neq 1$ always results in scale effects if the same model fluid is employed since only one of the relevant force ratios can be satisfied, whereas the remaining result in scale effects. However, scale effects are often negligibly small.
- Four approaches namely inspectional analysis, dimensional analysis, calibration and scale series are available to obtain model–prototype similarity, to quantify scale effects, to investigate how they affect the parameters and to establish limiting criteria where they can be neglected. Some of these approaches were applied on landslide generated impulse waves.
- Scale effects are minimized with three methods namely avoidance, compensation and correction. Examples illustrated how this is achieved for typical hydraulic flow phenomena.
- For each phenomenon or parameter in a model, the relative importance of the involved forces may vary and their tendency to cause scale effects depends on the prototype features relative to which they were defined. The correct definition of limiting criteria to avoid significant scale effects should therefore include the limitations and both the phenomenon and prototype features relative to which they were defined.
- Limiting criteria to avoid significant scale effects (Table 1) and typical scales of physical hydraulic models (Table 2) are presented.
- The avoidance of significant scale effects in models of hydraulic structures is in general straightforward with limiting criteria (Table 1). If the model is long, boundary friction also has to be modelled correctly. Obtaining model–prototype similarity is more challenging for movable bed models where the roughness and sediment properties have to be similar as well as the force ratios, or for fluid–structure interactions where the material properties have to be scaled. The investigation of such phenomena in hydraulic models without significant scale effects may not be possible.
- Despite the long tradition of physical hydraulic modelling, there exists, to the author's knowledge, no study where all relevant parameters were scaled to the miniature universe. This may be possible in future, for example, with numerical simulations.

Model and measurement effects are a further source of model–prototype deviations and have to be considered beside the herein addressed scale effects.

Acknowledgements

The author would like to thank Mr M.R. Hann for linguistic comments. Prof. W.H. Hager, Dr D. Stagonas and Mr D. Warbrick are acknowledged for helpful discussions.

Notation

a_M [L] = maximum wave amplitude
A_i [L^2] = cross-sectional area intake
b [L] = channel width
C [–] = Cauchy number
d_g [L] = grain diameter
d_j [L] = jet diameter
d_m [L] = mean grain diameter
d_{max} [L] = maximum grain diameter
d_{50} [L] = grain diameter at 50 wt%
d_{90} [L] = grain diameter at 90 wt%
E [–] = Euler number
E [$ML^{-1}T^{-2}$] = Young's modulus
F [–] = Froude number
F* [–] = grain Froude number
g [LT^{-2}] = gravitational acceleration
g' [LT^{-2}] = relative gravitational acceleration
h [L] = water depth
h_c [L] = critical flow depth
h_R [L] = run-up water layer thickness at still water level
Ka [–] = cavitation number
L [L] = characteristic length
m_s [M] = slide mass
n [–] = number of independent parameters
p [$ML^{-1}T^{-2}$] = pressure
p_v [$ML^{-1}T^{-2}$] = vapour pressure
p_0 [$ML^{-1}T^{-2}$] = absolute static pressure
q [divers] = independent parameter
Q_d [L^3T^{-1}] = design discharge
Q_i [L^3T^{-1}] = discharge intake
r [–] = number of reference dimension
R [–] = Reynolds number
R [L] = unlimited run-up height
R_c [L] = run-up height to crest of structure
R* [–] = grain Reynolds number
s [L] = slide thickness
S_E [–] = energy line slope
t [T] = time
T [T] = wave period
v^* [LT^{-1}] = shear velocity
V [LT^{-1}] = characteristic velocity
V_j [LT^{-1}] = jet velocity
V_R [LT^{-1}] = run-up velocity at still water level
V_0 [LT^{-1}] = velocity at specific location
$\forall_s$[L^3] = bulk slide volume
W [–] = Weber number
x [L] = horizontal distance from coordinate origin
z [L] = vertical distance from coordinate origin
z_i [L] = submergence depth intake
α [°] = slide impact angle
β, γ, δ [–] = exponents of reference parameters
η [L] = water surface displacement
λ [–] = scale ratio (inverse of scale 1 : λ)
μ [$ML^{-1}T^{-1}$] = dynamic viscosity
ν [L^2T^{-1}] = kinematic viscosity
Π [–] = parameters of Pi-theorem
ρ [ML^{-3}] = density
σ [MT^{-2}] = surface tension between air and water

Subscripts

c = critical
g = grain
H = height
I = impulse
M = model
P = prototype
s = sediment, slide
st = structure
1 = toe of hydraulic jump
2 = tailwater of hydraulic jump

References

Anwar, H.O., Weller, J.A., Amphlett, M.B. (1978). Similarity of free-vortex at horizontal intake. *J. Hydraulic Res*. 16(2), 95–105.

Boes, R.M. (2000). Scale effects in modelling two-phase stepped spillway flow. *Hydraulics of stepped spillways* 53–60, H.-E. Minor, W.H. Hager, eds. Rotterdam, Balkema.

Buckingham, E. (1914). On physically similar systems - Illustrations of the use of dimensional equations. *Physical Review* 4, 345–376.

Chanson, H. (1996). *Air bubble entrainment in free-surface turbulent shear flows*. Academic Press, San Diego.

Chanson, H. (2009). Turbulent air-water flows in hydraulic structures: Dynamic similarity and scale effects. *Environ. Fluid Mech*. 9(2), 125–142.

Cuomo, G., Allsop, W., Takahashi, S. (2010). Scaling wave impact pressures on vertical walls. *Coastal Engineering* 57(6), 604–609.

Ettema, R., Arndt, R., Roberts, P., Wahl, T. (2000). *Hydraulic modelling - Concepts and practice*. ASCE manuals and reports on engineering practice No. 97. ASCE, Reston VA.

Ettema, R., Kirkil, G., Muste, M. (2006). Similitude of large-scale turbulence in experiments on local scour at cylinders. *J. Hydraulic Eng*. 132(1), 33–40.

Fritz, H.M., Hager, W.H., Minor, H.-E. (2001). Lituya bay case: Rockslide impact and wave run-up. *Science of Tsunami Hazards* 19(1), 3–22.

Ghetti, A., D'Alpaos, L. (1977). Effets des forces de capillarité et de viscosité dans les écoulements permanents examinées en modèle physique (Effects of capillary and viscous forces in steady flows examined on physical model). 17th *IAHR Congress* Baden-Baden 2(A124), 389–396 [in French].

Hager, W.H., Bremen, R. (1989). Classical hydraulic jump: Sequent depths. *J. Hydraulic Res*. 27(5), 565–585.

Hager, W.H. (1994). Breitkroniger Überfall (Broad-crested weir). *Wasser Energie Luft* 86(11/12), 363–369 [in German].

Heller, V., Hager, W.H., Minor, H.-E. (2005). Ski jump hydraulics. *J. Hydraulic Eng*. 131(5), 347–355.

Heller, V. (2007). Massstabseffekte im hydraulischen Modell (Scale effects in hydraulic modelling). *Wasser Energie Luft* 99(2), 153–159 [in German].

Heller, V., Hager, W.H., Minor, H.-E. (2008). Scale effects in subaerial landslide generated impulse waves. *Exp. in Fluids* 44(5), 691–703.

Heller, V., Hager, W.H. (2010). Impulse product parameter in landslide generated impulse waves. *J. of Waterway, Port, Coastal and Ocean Engineering* 136(3), 145–155.

Huang, W., Yang, Q., Xiao, H. (2009). CFD modeling of scale effects on turbulence flow and scour around bridge piers. *Computers and Fluids* 38(5), 1050–1058.

Hughes, S.A. (1993). Advanced series on ocean engineering 7. *Physical models and laboratory techniques in coastal engineering*. World Scientific, London.

Ivicsics, L. (1978). *Hydraulic models*. Vizdok, Budapest.

Kamphuis, J.W. (1974). Practical scaling of coastal models. Proc. 14th *Coastal engineering conference*, Copenhagen 3, 2086–2101, ASCE, New York.

Keulegan, G.H. (1950). Wave motion. *Engineering hydraulics*, 711–768. H. Rouse, ed. Wiley, New York.

Kobus, H., ed. (1980). Hydraulic modelling. German association for water resources and land improvement, Bulletin 7. Parey, Hamburg.

Kundu, P.K., Cohen, I.M. (2004). *Fluid mechanics*. Academic Press, London.

Lauber, G., Hager, W.H. (1998). Experiments to dambreak wave: Horizontal channel. *J. Hydraulic Res*. 36(3), 291–307.

Le Méhauté, B. (1976). *An introduction to hydrodynamics and water waves*. Springer, New York.

Le Méhauté, B. (1990). Similitude. *Ocean engineering science, the sea*. B. Le Méhauté, D.M. Hanes, eds. Wiley, New York, 955–980.

Martin, H., Pohl, R., eds. (2000). *Technische Hydromechanik* 4 (Technical hydromechanics). Verlag für Bauwesen, Berlin [in German].

Maynord, S.T. (2006). Evaluation of the micromodel: An extremely small-scale movable bed model. *J. Hydraulic Eng*. 132(4), 343–353.

Miller, R.L. (1972). The role of surface tension in breaking waves. Proc. 13th *Coastal engineering conference*, Vancouver BC 1, 433–449. ASCE, New York.

Novak, P., Cabelka, J. (1981). *Models in hydraulic engineering*. Pitman, Boston.

Novak, P. (1984). Scaling factors and scale effects in modelling hydraulic structures. Symp. *Scale effects in modelling hydraulic structures* 0(3), 1–5. H. Rouse, ed. Technische Akademie, Esslingen.

Oliveto, G., Hager, W.H. (2005). Further results to time-dependent local scour at bridge elements. *J. Hydraulic Eng*. 131(2), 97–105.

Oumeraci, H. (1984). Scale effects in coastal hydraulic models. Symp. *Scale effects in modelling hydraulic structures* 7(10), 1–7. H. Kobus ed. Technische Akademie, Esslingen.

Raghunath, H.M. (1967). *Dimensional analysis and hydraulic model testing*. Asia Publishing House, London.

Ranieri, G. (2007). The surf zone distortion of beach profiles in small-scale coastal models. *J. Hydraulic Res*. 45(2), 261–269.

Rouse, H., Siao, T.T., Nagaratnam, S. (1959). Turbulence characteristics of the hydraulic jump. *Trans. ASCE* 124, 926–966.

Rutschmann, P. (1988). Belüftungseinbauten in Schussrinnen (Chute aerators). *VAW Mitteilung* 97. D. Vischer ed. ETH Zurich, Zürich [in German].

Schmocker, L., Hager, W.H. (2009). Modelling dike breaching due to overtopping. *J. Hydraulic Res*. 47(5), 585–597.

Schüttrumpf, H., Oumeraci, H. (2005). Scale and model effects in crest level design. Proc. 2nd. *Coastal Symposium,* 1–12. Höfn, Iceland.

Skladnev, M.F., Popov, I.Y. (1969). Studies of wave loads on concrete slope protections of earth dams. Symp. *Research on wave action* 2(7), 1–11 Delft Hydraulics Laboratory, Delft NL.

Spurk, J.H. (1992). *Dimensionsanalyse in der Strömungslehre* (Dimensional analysis in fluid flow). Springer, Berlin [in German].

Stagonas, D. (2010). Micro-modelling of wave fields. *PhD thesis*. University of Southampton, Southampton.

Stagonas, D., Müller, G., Warbrick, D., Magagna, D. (2010). Surface tension effects in small-scale laboratory breaking waves. Proc. *Coastlab* 10. Barcelona, Spain [accepted].

Taylor, R.N., ed. (1995). *Geotechnical centrifuge technology*. Chapman and Hall, Glasgow.

Webb, C.B., Barfuss, S.L., Johnson, M.C. (2010). Modelling roughness in scale models. *J. Hydraulic Res*. 48(2), 260–264.

Weichert, R. (2006). Bed morphology and stability of steep open channels. *VAW Mitteilung* 192. H.-E. Minor ed., ETH Zurich, Zürich.

Yalin, M.S. (1971). *Theory of hydraulic models*. Macmillan, London.

Zarn, B. (1992). Lokale Gerinneaufweitung: Eine Massnahme zur Sohlenstabilisierung der Emme bei Utzenstorf (Local river expansion: A measure to stabilize the bed of Emme River at Utzendorf). *VAW Mitteilung* 118. D. Vischer ed. ETH Zurich, Zürich [in German].